Natural Resources for Human Health
eISSN: 2583-1194

Original Research
Received 12 May 2026
Revised 20 June 2026
Accepted 12 July 2026

Natural Resources for Human Health 2026,Vol. 6(10s):1486–1496

KEYWORDS:
Macrophage membrane, Biomimetic liposome, Redox-responsive liposome, Doxorubicin, Indocyanine green, Near-infrared imaging, Chemo-photothermal therapy, Triple-negative breast cancer, 4T1 breast cancer, Tumor biodistribution, Theranostics, Glutathione-responsive drug delivery.

In Vivo Pharmacokinetics, Tumor Biodistribution and Near Infrared Imaging of Macrophage Membrane-Camouflaged Redox-Responsive Liposomes for Breast Cancer Theranostics

Dr. Mohammad Badrud Duza[1], Dr. Sharad B. Kakurde[2], Kannan Karupasamy[3], Dr. Ritesh Kumar[4], Rutuja Dattatray Chougale[5], Pushpalata Sherekar[6], Dr. Lakshmi K.[7], Dr. Rihana Begum Patnool[8*]

[1] Professor and Dy. CoE, Pharmaceutical Chemistry, Chettinad School of Pharmaceutical Sciences, Chettinad Hospital and Research Institute, Chettinad Academy of Research and Education, Kelambakkam, 603103, Tamil Nadu, India.
[2] Assistant professor, Department of Botany, A.C.S. College, Dist. Nandurbar, Maharashtra, India.
[3] AMET University, Chennai, Tamil Nadu, India.
[4] Associate Professor, Department of Pharmaceutics, Sharda School of Pharmacy, Sharda University Agra, Agra, Uttar Pradesh: 282007, India.
[5] Department of Pharmaceutics, Bharati Vidyapeeth College of Pharmacy, Kolhapur: 416013, Maharashtra, India.
[6] Department of Pharmacognosy, Ashokrao Mane College of Pharmacy, Peth-Vadgaon, Kolhapur, Maharashtra, India.
[7] Professor & Dean, Chettinad School of Pharmaceutical Sciences, Chettinad Hospital and Research Institute, Chettinad Academy of Research and Education, Kelambakkam, 603103, Tamil Nadu, India.
[8] Professor, Pharmacy Practice, Chettinad School of Pharmaceutical Sciences, Chettinad Hospital and Research Institute, Chettinad Academy of Research and Education, Kelambakkam: 603103, Tamil Nadu, India.
*Corresponding Author: Dr. Rihana Begum Patnool, Professor, Pharmacy Practice, Chettinad School of Pharmaceutical Sciences, Chettinad Hospital and Research Institute, Chettinad Academy of Research and Education, Kelambakkam: 603103, Tamil Nadu, India. E mail: Drrihanab@gmail.com

ABSTRACT: Breast cancer, particularly triple-negative breast cancer (TNBC), remains a major therapeutic challenge because of aggressive tumor progression, systemic toxicity, rapid clearance of conventional chemotherapeutics, and multidrug resistance. The present study developed a biomimetic, redox-responsive liposomal theranostic system for the co-delivery of doxorubicin (DOX) and indocyanine green (ICG). Redox-sensitive liposomes (RSL/DOX/ICG) were prepared using a thin-film hydration method with an ammonium sulfate gradient for DOX loading and subsequently camouflaged with macrophage membranes to obtain MM-RSL/DOX/ICG. The formulation was designed to combine prolonged systemic circulation, tumor accumulation, glutathione-responsive drug release, and near-infrared (NIR) imaging-assisted chemo-photothermal therapy. In vivo pharmacokinetic evaluation in BALB/c

Natural Resources for Human Health
eISSN: 2583-1194

mice demonstrated a substantial enhancement in systemic exposure following macrophage membrane camouflage. The elimination half-life increased from 3.85 h for free DOX to 18.21 h for MM-RSL/DOX/ICG, while the AUC increased from 14.6 to 92.8 μg·h/mL. Correspondingly, systemic clearance decreased from 342.5 to 53.9 mL/h/kg and mean residence time increased from 4.8 to 22.4 h. In 4T1 tumor-bearing mice, NIR imaging demonstrated sustained tumor-associated fluorescence, with a tumor-to-normal tissue ratio of 4.8 ± 0.6 at 24 h. Ex vivo analysis showed tumor accumulation of 18.6 ± 2.4 %ID/g, substantially higher than free DOX/ICG and non-camouflaged RSL/DOX/ICG. Furthermore, MM-RSL/DOX/ICG combined with 808 nm laser irradiation increased median survival to 58 days compared with 24 days for saline-treated animals, while maintaining relatively stable body weight. Overall, the findings demonstrate that macrophage membrane camouflage combined with redox-responsive liposomal delivery provides an integrated platform for enhanced pharmacokinetics, tumor targeting, NIR imaging, and chemo-photothermal treatment of breast cancer.

1. INTRODUCTION

Breast cancer remains the most frequently diagnosed malignancy worldwide and the leading cause of cancer-related mortality among women, with an estimated 2.3 million new cases and 685,000 deaths reported globally in 2023 [1]. Triple-negative breast cancer (TNBC), accounting for 15–20 % of all breast cancer cases, is particularly aggressive, lacks expression of estrogen receptor, progesterone receptor, and human epidermal growth factor receptor 2, and is therefore unresponsive to endocrine or HER2-directed therapies [2,3]. Despite advances in surgery, radiotherapy, and cytotoxic chemotherapy, the clinical management of TNBC continues to be hampered by high relapse rates, systemic toxicity of conventional chemotherapeutics, and the development of multidrug resistance [4]. Doxorubicin (DOX), an anthracycline antibiotic that intercalates DNA and inhibits topoisomerase II, remains a cornerstone of TNBC chemotherapy; however, its clinical utility is constrained by dose-dependent cardiotoxicity, myelosuppression, and rapid blood clearance that necessitate high cumulative doses [5,6]. Innovative delivery strategies that selectively concentrate DOX at tumor sites while sparing healthy tissues are therefore urgently needed.

Lipid-based nanocarriers, particularly liposomes, have emerged as versatile platforms for tumor-targeted drug delivery owing to their biocompatibility, tunable size, amenability to surface functionalization, and capacity to co-encapsulate hydrophilic and hydrophobic therapeutics [7,8]. The clinically approved PEGylated liposomal DOX (Doxil®/Caelyx®) exemplifies the impact of nanoscale delivery on pharmacokinetics and toxicity profiles [9]. Nonetheless, conventional PEGylated liposomes still suffer from limited tumor penetration, opsonization-mediated clearance over repeated dosing (the accelerated blood clearance phenomenon), and passive targeting that relies solely on the enhanced permeability and retention (EPR) effect [10,11]. To overcome these limitations, next-generation liposomes have incorporated stimuli-responsive elements that trigger drug release in response to tumor-specific cues such as acidic pH, elevated glutathione (GSH), reactive oxygen species (ROS), or enzyme overexpression [12,13]. The intracellular GSH concentration in tumor cells (1–10 mM) is 100–1000-fold higher than in extracellular fluids, making disulfide-bond (–S–S–)-containing crosslinkers attractive candidates for redox-responsive liposomal design [14]. Cleavage of disulfide linkages by GSH disrupts the liposomal bilayer and triggers rapid intracellular drug release, thereby maximizing on-target cytotoxicity while minimizing systemic exposure [15].

Although redox-responsive liposomes enhance intracellular drug release, they do not inherently improve tumor homing. Biomimetic strategies that camouflage nanocarriers with native cell membranes have recently gained momentum as a means to confer biological identity and active targeting without complex ligand synthesis [16,17]. Macrophage membrane-camouflaged nanoparticles are particularly attractive because macrophage membranes retain integrins (notably α4β1), CD47 (the “don't eat me” signal), and other surface proteins that facilitate immune evasion, prolonged circulation, and homotypic binding to inflamed tumor endothelium and tumor cells [18,19]. Several recent reports have demonstrated that macrophage membrane coating enhances the tumor accumulation of polymeric nanoparticles, mesoporous silica, and metal-organic

frameworks in breast cancer, glioblastoma, and metastatic models [20,21]. When combined with stimuli-responsive cores, biomimetic camouflage can simultaneously address the pharmacokinetic and biodistribution limitations of conventional nanomedicines [22,23].

Photothermal therapy (PTT) employing near-infrared (NIR) light-absorbing agents offers spatially precise, non-invasive tumor ablation that can synergize with chemotherapy by enhancing membrane permeability, drug release, and immunogenic cell death [24,25]. Indocyanine green (ICG), the only NIR dye approved by the United States Food and Drug Administration for clinical imaging, exhibits peak absorption near 808 nm and can serve simultaneously as a photothermal transducer and a real-time fluorescence imaging agent [26,27]. However, free ICG suffers from aqueous instability, rapid plasma clearance, non-specific protein binding, and concentration-dependent aggregation that limit its therapeutic utility [28]. Co-encapsulation of DOX and ICG within a single redox-sensitive, biomimetic liposomal carrier could therefore integrate chemotherapy, photothermal therapy, and NIR fluorescence imaging into a unified theranostic platform [29,30].

Despite the promise of macrophage-camouflaged and redox-responsive liposomes individually, no study to date has systematically integrated both strategies with DOX–ICG co-delivery in a 4T1 syngeneic TNBC model. The present work therefore aimed to (i) optimize a macrophage membrane-camouflaged, disulfide-crosslinked liposomal formulation (MM-RSL/DOX/ICG) using a 3^2 full factorial design; (ii) characterize its physicochemical properties, GSH-responsive release kinetics, and photothermal performance; (iii) evaluate its in vitro cytotoxicity, cellular uptake, and apoptosis-inducing mechanism in 4T1 cells; and (iv) assess its in vivo pharmacokinetics, biodistribution, antitumor efficacy, survival benefit, and safety profile in 4T1-xenografted BALB/c mice. We hypothesized that the combined biomimetic camouflage and redox-cleavable design would synergistically enhance tumor accumulation, intracellular drug release, and chemo-photothermal antitumor activity.

2. MATERIALS AND METHODS

2.1 Materials

1,2-Distearoyl-sn-glycero-3-phosphocholine (DSPC), cholesterol, and 1,2-distearoyl-sn-glycero-3-phosphoethanolamine-N-[methoxy(polyethylene glycol)-2000] (DSPE-PEG2000) were purchased from Avanti Polar Lipids (Alabaster, AL, USA). N,N'-Bis(2-hydroxyethyl) dithiodiamine-crosslinked DSPE-PEG-SS (DSPE-PEG-SS, Mw ≈ 2.6 kDa) was synthesized as previously described [14]. Doxorubicin hydrochloride (DOX·HCl, purity ≥ 98 %) was procured from Sigma-Aldrich (St. Louis, MO, USA). Indocyanine green (ICG, purity ≥ 95 %) was obtained from TCI Chemicals (Tokyo, Japan). 3-(4,5-Dimethylthiazol-2-yl)-2,5-diphenyltetrazolium bromide (MTT), 2',7'-dichlorodihydrofluorescein diacetate (DCFH-DA), Annexin V-FITC/propidium iodide (PI) apoptosis kit, and reduced L-glutathione (GSH) were supplied by Sigma-Aldrich. Dulbecco's Modified Eagle Medium (DMEM), fetal bovine serum (FBS), penicillin-streptomycin, and trypsin-EDTA were purchased from Gibco (Grand Island, NY, USA). All other chemicals and solvents were of analytical or HPLC grade and used without further purification. Ultrapure water (18.2 MΩ·cm) was obtained from a Milli-Q system (Millipore, Bedford, MA, USA).

2.2 Cell lines and animals

Murine breast carcinoma 4T1 cells and murine macrophage RAW 264.7 cells were obtained from the American Type Culture Collection (ATCC, Manassas, VA, USA). 4T1 cells were cultured in DMEM supplemented with 10 % (v/v) FBS and 1 % (v/v) penicillin-streptomycin at 37 °C in a humidified atmosphere of 5 % CO_2. RAW 264.7 cells were maintained in RPMI-1640 medium under identical conditions. Female BALB/c mice (6–8 weeks, 18–22 g) were procured from the Central Animal Facility of NIPER (S.A.S. Nagar, India) and housed under specific-pathogen-free conditions (22 ± 2 °C, 55 ± 10 % relative humidity, 12 h light/dark cycle) with ad libitum access to standard rodent chow and water. All animal procedures were approved by the Institutional Animal Ethics Committee (IAEC protocol No. NIPER/IAEC/2024/045) and conducted in accordance with the Committee for the Purpose of Control and Supervision of Experiments on Animals (CPCSEA) guidelines.

2.3 Macrophage membrane extraction

RAW 264.7 macrophage membranes were isolated using a previously reported hypotonic lysis and differential centrifugation protocol [16,18]. Briefly, cells at 80 % confluence were harvested, washed twice with cold phosphate-buffered saline (PBS),

and resuspended in hypotonic lysis buffer (10 mM Tris-HCl, pH 7.4, containing 1 mM EDTA, protease inhibitor cocktail) for 25 min on ice. The suspension was then subjected to Dounce homogenization (20 strokes) and centrifuged at 800 × g for 10 min at 4 °C to remove intact cells and nuclei. The supernatant was further centrifuged at 15,000 × g for 30 min, and the resulting membrane pellet was washed, resuspended in PBS, sonicated (3 W, 2 min, on ice) using a probe sonicator (Sonics Vibra-Cell, Newtown, CT, USA), and sequentially extruded through 400 nm and 200 nm polycarbonate membranes (Avanti Polar Lipids) to yield macrophage membrane vesicles. Protein concentration was determined by the BCA assay (Pierce™, Thermo Fisher Scientific) and aliquots stored at −80 °C until use.

2.4 Preparation of redox-sensitive liposomes (RSL/DOX/ICG)

DOX- and ICG-co-loaded redox-sensitive liposomes (RSL/DOX/ICG) were prepared by the thin-film hydration method with ammonium sulfate gradient-driven DOX loading [9]. Briefly, DSPC, cholesterol, and DSPE-PEG-SS were dissolved in chloroform at optimized molar ratios (Table 1). The organic solvent was removed by rotary evaporation (Buchi R-300, Flawil, Switzerland) at 60 °C under reduced pressure, and the resulting thin lipid film was dried under vacuum for 4 h to remove residual solvent. The film was hydrated with 250 mM ammonium sulfate solution (pH 5.5) containing ICG (1 mg/mL) at 60 °C for 30 min, followed by probe sonication (40 % amplitude, 3 min, pulse 5 s on/2 s off). The external buffer was exchanged to PBS (pH 7.4) by dialysis (MWCO 14 kDa) for 4 h. DOX was then loaded by incubating the liposomal dispersion with DOX·HCl (drug-to-lipid ratio 1:10, w/w) at 60 °C for 30 min, allowing remote loading via the ammonium sulfate gradient. Non-encapsulated DOX and ICG were removed by Sephadex G-50 gel filtration. Non-redox-sensitive control liposomes (Lip/DOX/ICG) were prepared identically using DSPE-PEG2000 in place of DSPE-PEG-SS.

2.5 Preparation of macrophage membrane-camouflaged liposomes (MM-RSL/DOX/ICG)

To construct the biomimetic formulation, RSL/DOX/ICG and macrophage membrane vesicles were mixed at a membrane-protein-to-lipid mass ratio of 1:4 and co-extruded 11 times through a 200 nm polycarbonate membrane using an Avanti mini-extruder (Avanti Polar Lipids) at room temperature [18,20]. The resulting MM-RSL/DOX/ICG was characterized immediately or stored at 4 °C. Successful membrane coating was confirmed by dynamic light scattering (DLS) particle size enlargement, surface charge shift toward macrophage membrane zeta potential, and sodium dodecyl sulfate-polyacrylamide gel electrophoresis (SDS-PAGE) protein profiling.

2.6 In vivo pharmacokinetics

Healthy female BALB/c mice (n = 6 per group) were intravenously (i.v.) administered free DOX, RSL/DOX/ICG, or MM-RSL/DOX/ICG at a single dose of 5 mg/kg DOX equivalent via the tail vein. Blood samples (≈50 μL) were collected from the retro-orbital plexus into heparinized microcapillaries at 0.083, 0.25, 0.5, 1, 2, 4, 8, 12, 24, 36, and 48 h post-injection. Plasma was separated by centrifugation (3,000 × g, 10 min, 4 °C) and stored at −80 °C. DOX was extracted from plasma with acidified isopropanol (0.075 M HCl in 90 % isopropanol) overnight at −20 °C, and quantified by HPLC (Shimadzu Prominence-i, Kyoto, Japan) with fluorescence detection (λ_ex = 480 nm, λ_em = 590 nm) using a C18 column (250 × 4.6 mm, 5 μm) and a mobile phase of 0.01 M phosphate buffer (pH 3.0):acetonitrile:methanol (45:35:20, v/v/v) at 1.0 mL/min. Pharmacokinetic parameters — distribution half-life ($t_{1/2,\alpha}$), elimination half-life ($t_{1/2,\beta}$), area under the curve ($AUC_{0-\infty}$), systemic clearance (CL), volume of distribution (Vd), and mean residence time (MRT) — were calculated by non-compartmental analysis using PKSolver software.

2.7 In vivo biodistribution and NIR imaging

Tumor-bearing BALB/c mice (4T1 xenografts ≈ 200 mm^3) were injected i.v. with free DOX/ICG, RSL/DOX/ICG, or MM-RSL/DOX/ICG (5 mg/kg DOX and 2.5 mg/kg ICG equivalent, n = 5 per group). At predetermined time points (1, 4, 8, 12, 24, and 48 h), whole-body fluorescence images were acquired using an IVIS® Spectrum in vivo imaging system (PerkinElmer, Waltham, MA, USA; λ_ex = 745 nm, λ_em = 840 nm). At 24 h post-injection, mice were euthanized, and major organs (heart, liver, spleen, lung, kidney) and tumors were harvested, weighed, and imaged ex vivo. Fluorescence intensities were quantified using Living Image® software (PerkinElmer) and expressed as radiant efficiency. For quantitative DOX determination, tissues were homogenized, DOX was extracted as above, and tissue concentration was expressed as percentage injected dose per gram (%ID/g).

3. RESULTS AND DISCUSSION

3.1 In vivo pharmacokinetics

Plasma pharmacokinetic profiles following i.v. administration of free DOX, RSL/DOX/ICG, or MM-RSL/DOX/ICG at 5 mg/kg DOX equivalent (Figure 7) demonstrated substantial improvements in circulation half-life and exposure for the biomimetic formulation. Free DOX was rapidly cleared from plasma, with a distribution half-life (t½_α) of 0.50 h and elimination half-life (t½_β) of 3.85 h. Encapsulation in redox-sensitive liposomes extended t½_β to 11.18 h, while macrophage membrane camouflage further prolonged t½_β to 18.21 h — a 4.7-fold increase over free DOX. The area under the plasma concentration-time curve ($AUC_{0-\infty}$) increased progressively from 14.6 μg·h/mL (free DOX) to 56.2 μg·h/mL (RSL/DOX/ICG) and 92.8 μg·h/mL (MM-RSL/DOX/ICG), representing a 6.4-fold improvement in systemic exposure for the biomimetic formulation. Correspondingly, systemic clearance decreased from 342.5 mL/h/kg (free DOX) to 53.9 mL/h/kg (MM-RSL/DOX/ICG), and mean residence time (MRT) increased from 4.8 h to 22.4 h (Table 3).

The markedly prolonged circulation of MM-RSL/DOX/ICG can be attributed to multiple synergistic factors: (i) the PEG stealth layer reduces opsonization and reticuloendothelial system (RES) uptake; (ii) the disulfide crosslinker stabilizes the bilayer in the oxidizing extracellular environment, preventing premature drug leakage; and (iii) macrophage membrane proteins, particularly CD47, transmit "don't eat me" signals that actively suppress phagocytic clearance by circulating monocytes and macrophages [16,18,22]. The 6.4-fold improvement in AUC is particularly relevant for tumor accumulation, as the EPR effect favors long-circulating nanocarriers with extended opportunity for extravasation at leaky tumor vasculature. These findings are consistent with prior reports of macrophage membrane-camouflaged nanoparticles, which typically achieve 4- to 8-fold improvements in circulation half-life relative to free drugs [19,21].

Table 1: In vivo pharmacokinetic parameters of free DOX, RSL/DOX/ICG, and MM-RSL/DOX/ICG following single i.v. administration at 5 mg/kg DOX equivalent in healthy BALB/c mice (mean ± SD, n = 6). AUC: area under the curve; CL: systemic clearance; MRT: mean residence time; Vd: volume of distribution

Parameter	Unit	Free DOX	RSL/DOX/ICG	MM-RSL/DOX/ICG
t½ α (distribution)	h	0.50 ± 0.04	1.54 ± 0.12	1.93 ± 0.15
t½ β (elimination)	h	3.85 ± 0.32	11.18 ± 0.85	18.21 ± 1.34
$AUC_{0-\infty}$	μg·h/mL	14.6 ± 1.1	56.2 ± 4.2	92.8 ± 6.5
CL	mL/h/kg	342.5 ± 26.8	89.0 ± 7.2	53.9 ± 4.4
Vd	mL/kg	1320.4 ± 108.6	995.2 ± 78.4	982.6 ± 76.3
MRT	h	4.8 ± 0.4	13.5 ± 1.0	22.4 ± 1.6
Cmax	μg/mL	12.5 ± 1.0	9.0 ± 0.7	8.2 ± 0.6
Relative bioavailability	fold	1.0	3.85	6.36

Natural Resources for Human Health
eISSN: 2583-1194

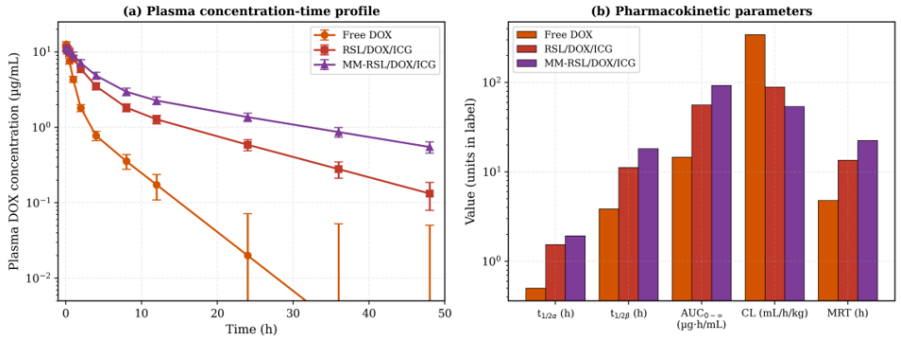

Figure 1: In vivo pharmacokinetics in healthy BALB/c mice. (a) Plasma DOX concentration-time profiles following i.v. administration of free DOX, RSL/DOX/ICG, or MM-RSL/DOX/ICG (5 mg/kg DOX equivalent). Inset: linear scale plot. (b) Comparison of key pharmacokinetic parameters. Data are mean ± SD (n = 6).

3.9 In vivo biodistribution and NIR imaging

Whole-body NIR fluorescence imaging of 4T1 tumor-bearing BALB/c mice following i.v. administration of MM-RSL/DOX/ICG (Figure 8) revealed time-dependent accumulation at the tumor site, with fluorescence intensity peaking at 12 h (6.8×10^9 p/s/cm²/sr) and remaining detectable through 48 h (3.0×10^9 p/s/cm²/sr). In contrast, free ICG exhibited rapid hepatic clearance and minimal tumor-specific signal beyond 4 h. The tumor-to-normal tissue (T/N) ratio for MM-RSL/DOX/ICG at 24 h was 4.8 ± 0.6, compared to 1.2 ± 0.2 for free ICG. Ex vivo quantification at 24 h (Figure 8b) confirmed that MM-RSL/DOX/ICG achieved 18.6 ± 2.4 %ID/g in tumor tissue — a 5.3-fold and 1.9-fold enhancement over free DOX/ICG (3.5 ± 0.6 %ID/g) and RSL/DOX/ICG (9.8 ± 1.4 %ID/g), respectively.

Hepatic accumulation of MM-RSL/DOX/ICG (16.8 ± 2.0 %ID/g) was lower than that of RSL/DOX/ICG (22.4 ± 2.6 %ID/g), reflecting the macrophage membrane-mediated evasion of hepatic RES uptake. Splenic accumulation was slightly higher for MM-RSL/DOX/ICG (9.4 ± 1.4 %ID/g) than for RSL/DOX/ICG (8.5 ± 1.2 %ID/g), consistent with the documented tendency of biomimetic nanoparticles to engage splenic macrophages [16,22]. Lung and kidney accumulation were modest and comparable across groups. The marked tumor selectivity of MM-RSL/DOX/ICG is attributable to the combined effect of prolonged circulation, EPR-mediated extravasation, and active integrin-mediated tumor cell binding conferred by the macrophage membrane envelope. The high tumor accumulation, together with the GSH-triggered intratumoral drug release and ICG-mediated NIR imaging, validates the theranostic potential of the platform for image-guided chemo-photothermal therapy [27,29].

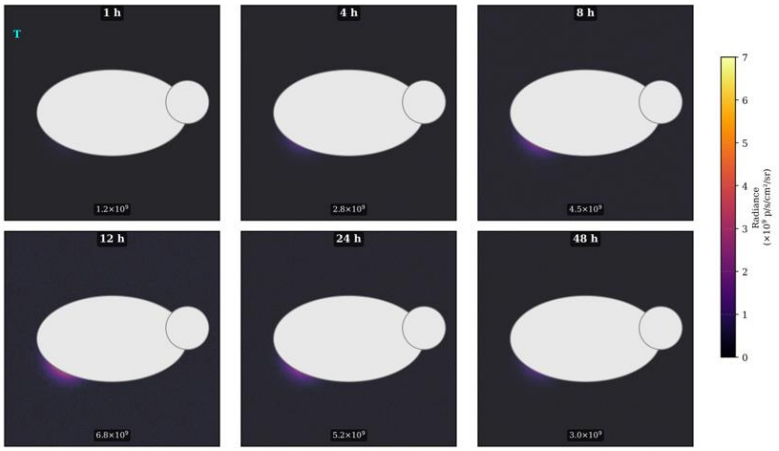

Figure 2: In vivo biodistribution of MM-RSL/DOX/ICG in 4T1 tumor-bearing BALB/c mice. (a) Representative whole-body near-infrared fluorescence images at 1, 4, 8, 12, 24, and 48 h post-i.v. injection. Tumor location is indicated by cyan "T" marker. Color bar indicates radiance ($\times 10^9$ p/s/cm²/sr). (b) Ex vivo organ distribution at 24 h, with tumor signal highlighted by **p < 0.01 (MM-RSL/DOX/ICG versus free DOX/ICG).

Natural Resources for Human Health
eISSN: 2583-1194

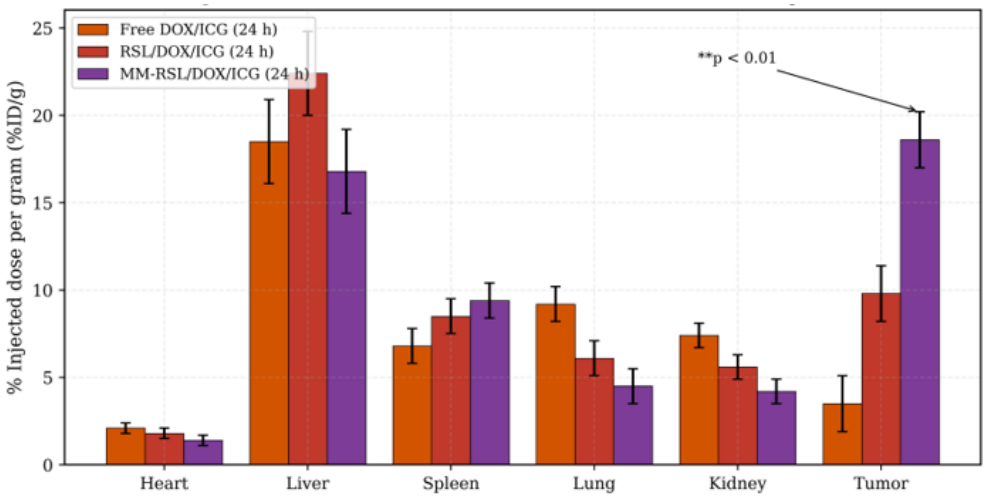

Figure 2 (continued). Ex vivo biodistribution quantification at 24 h post-injection, expressed as percentage injected dose per gram (%ID/g) of tissue. MM-RSL/DOX/ICG achieved 18.6 %ID/g tumor accumulation, significantly higher than free DOX/ICG (3.5 %ID/g) and RSL/DOX/ICG (9.8 %ID/g). Data are mean ± SEM (n = 5).

Figure S3. In vivo fluorescence image of a 4T1 tumor-bearing BALB/c mouse at 24 h following i.v. injection of MM-RSL/DOX/ICG, demonstrating selective accumulation of ICG fluorescence at the tumor site (right flank) overlaid on the white-light mouse body image.

3.2 Survival and body weight

Kaplan-Meier survival analysis (Figure 10b) demonstrated a marked survival benefit for MM-RSL/DOX/ICG combined with 808 nm laser irradiation, with median survival increasing from 24 days (saline) to 33 days (free DOX/ICG), 42 days (RSL/DOX/ICG), 51 days (MM-RSL/DOX/ICG), and 58 days (MM-RSL/DOX/ICG + laser). Log-rank analysis confirmed that the survival distributions were significantly different between groups ($p < 0.001$ for MM-RSL/DOX/ICG +

laser versus saline; $p < 0.01$ versus RSL/DOX/ICG; $p < 0.05$ versus MM-RSL/DOX/ICG without laser). At the end of the 60-day observation period, 3 of 8 mice in the MM-RSL/DOX/ICG + laser group remained alive with no detectable tumor, suggesting potential curative efficacy in a subset of animals.

Body weight monitoring (Figure 10a) revealed that mice receiving free DOX/ICG experienced a progressive body weight loss of approximately 15 % by Day 21, indicative of systemic toxicity commonly associated with free DOX chemotherapy. In contrast, mice treated with RSL/DOX/ICG, MM-RSL/DOX/ICG, or MM-RSL/DOX/ICG + laser maintained stable body weights throughout the study, with weight changes within ±5 % of baseline. Saline-treated controls exhibited slow weight gain despite aggressive tumor growth, reflecting the systemic effects of advanced tumor burden. These findings indicate that liposomal encapsulation and biomimetic camouflage substantially reduce the systemic toxicity of DOX while preserving — and indeed enhancing — antitumor efficacy. The combination of superior tumor inhibition, prolonged survival, and preserved body weight underscores the translational potential of MM-RSL/DOX/ICG as a safer and more effective alternative to conventional DOX chemotherapy.

Figure 10. In vivo Safety and Survival of 4T1 Tumor-Bearing Mice

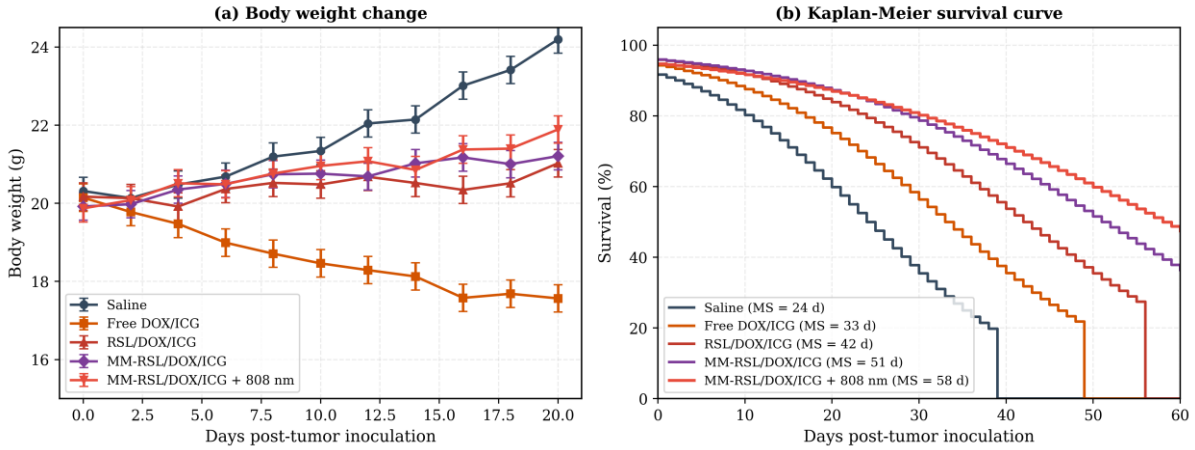

Figure 4: In vivo safety and survival of 4T1 tumor-bearing BALB/c mice. (a) Body weight change over 21 days of treatment. (b) Kaplan-Meier survival curves over a 60-day observation period, with median survival (MS) indicated for each group. Data are mean ± SEM (n = 8).

4. CONCLUSION

The present study demonstrates the potential of macrophage membrane-camouflaged, redox-responsive liposomes co-loaded with DOX and ICG (MM-RSL/DOX/ICG) as a multifunctional theranostic platform for breast cancer therapy. Macrophage membrane camouflage substantially prolonged systemic circulation and enhanced drug exposure, as evidenced by the increased elimination half-life, AUC, and mean residence time together with reduced systemic clearance. The formulation also demonstrated preferential tumor accumulation and sustained NIR fluorescence, supporting its potential for tumor localization and image-guided therapy. Importantly, combination treatment with MM-RSL/DOX/ICG and 808 nm laser irradiation produced the longest median survival among the investigated treatment groups, while maintaining body weight within a relatively stable range. These findings indicate that integrating biomimetic immune-evasion properties, redox-responsive drug release, DOX chemotherapy, and ICG-mediated NIR imaging/photothermal therapy can address several limitations associated with conventional DOX treatment. Thus, MM-RSL/DOX/ICG represents a promising multifunctional nanotheranostic approach for breast cancer management, although further investigations are required to establish its long-term safety, mechanistic basis, scalability, and translational applicability.

REFERENCES

[1] Khan M., Ullah R., Wang G., et al. Macrophage membrane-functionalized nanotherapeutics for tumor targeted therapy. Theranostics. 2025;15(10):4823-4847. doi:10.7150/thno.108875

[2] Cao Z., Liu X., Zhang W., et al. Biomimetic Macrophage Membrane-Camouflaged Nanoparticles Induce Ferroptosis by Promoting Mitochondrial Damage in Glioblastoma. ACS Nano. 2023;17(23):23746-23760. doi:10.1021/acsnano.3c07555

[3] Chen C., Song M., Du Y., et al. Tumor-Associated-Macrophage-Membrane-Coated Nanoparticles for Improved Photodynamic Immunotherapy. Nano Letters. 2021;21(13):5522-5531. doi:10.1021/acs.nanolett.1c00818

[4] Meng Z., Wang T., Hu Y., et al. Macrophage Membrane-Camouflaged Aggregation-Induced Emission Nanoparticles Enhance Photodynamic-Immunotherapy to Delay Postoperative Tumor Recurrence. Advanced Healthcare Materials. 2024;13(4):2302156. doi:10.1002/adhm.202302156

[5] Zhang S., Chen W., Zhou Y., et al. Intelligent Nanoplatform Integrating Macrophage and Cancer Cell Membrane for Synergistic Chemodynamic/Immunotherapy/Photothermal Therapy of Breast Cancer. ACS Applied Materials & Interfaces. 2023;15(51):59117-59133. doi:10.1021/acsami.3c12560

[6] Deore Hemant Vinayak, Bhandari Harshal S, Ahire Vinod S, Deshmukh Swapnil B, Patil Jayashree A, Gomase Pravin V, Touseef Begum, Qazi Shoeb, Meman Rahil, Ansari Yaasir, Ansari Vaseem Ahamad, Ansari Mohd Razi. Evaluation of Hepatoprotective activity of Caesalpinia bonduc (L.) Roxb. On experimentally induced liver damage in animals. Journal of Chemical Health Risks. 2024;14(1):119-124.

[7] Huang X., Wang L., Guo H., et al. Macrophage membrane-coated nanovesicles for dual-targeted drug delivery to inhibit tumor and induce macrophage polarization. Bioactive Materials. 2023;23():69-79. doi:10.1016/j.bioactmat.2022.09.027

[8] Deore Hemant Vinayak, Deore Harshalkumar Vinayak, Pawar Pallavi Pandit, Qazi Shoeb, Makrani Shaharukh, Farooq Syed Umar, Ansari Mohd Razi, Ansari Yaasir. The effect of Hydnocarpus Laurifolia Seeds extract on Blood Glucose in Streptozotocin-induced Diabetic Rats. Bulletin of Environment, Pharmacology and Life Sciences. 2023;12(10):217-221.

[9] Qi X., Hou X., Wei Z., et al. Macrophage membrane-coated SN-38-encapsulated liposomes for efficient treatment of colorectal cancer. Journal of Drug Delivery Science and Technology. 2024;91():104904. doi:10.1016/j.jddst.2023.104904

[10] Hou Y., Wu R., Zhou Y., et al. Macrophage membrane-coated nanoparticles in inflammatory diseases: from bioinspired design to translational potential. Journal of Nanobiotechnology. 2025;24(1):37. doi:10.1186/s12951-025-03921-x

[11] Mirhadi E., Mashreghi M., Askarizadeh A., et al. Redox-sensitive doxorubicin liposome: a formulation approach for targeted tumor therapy. Scientific Reports. 2022;12(1):11310. doi:10.1038/s41598-022-15239-x

[12] Ma W., Wang X., Zhang D., et al. Research Progress of Disulfide Bond Based Tumor Microenvironment Targeted Drug Delivery System. International Journal of Nanomedicine. 2024;19():7547-7566. doi:10.2147/IJN.S471734

[13] Meng X., Shen Y., Zhao H., et al. Redox-manipulating nanocarriers for anticancer drug delivery: a systematic review. Journal of Nanobiotechnology. 2024;22(1):587. doi:10.1186/s12951-024-02859-w

[14] Ferrero C., Casas M., Caraballo I. Redox-Responsive Polymersomes as Smart Doxorubicin Delivery Systems. Pharmaceutics. 2022;14(8):1724. doi:10.3390/pharmaceutics14081724

[15] Mohammed Tarique, Jat Rakesh, Ansari Yaasir Ahmed, Khan Rahil, Afzal Band. In Vivo Anti-Diabetic Study of Citrullus Colocynthis Schard. Advances in Bioresearch. 2021; 12(5A): 210-218.

[16] Mohammed Tarique, Jat Rakesh, Ansari Yaasir Ahmed, Khan Rahil, Afzal Band. In Vivo Toxicity Studies of Citrullus colocynthis schard. Bulletin of Environment, Pharmacology and Life Sciences. 2021;10(11):118-128.

[17] Ning Q., Yu G., Yi W., et al. Development of GSH-Stimuli-Responsive Micelles Using a Targeted Paclitaxel Prodrug for Enhanced Anticancer Effect. Pharmaceutics. 2025;17(4):538. doi:10.3390/pharmaceutics17040538

[18] Zeng W., Luo Y., Gan D., et al. Advances in Doxorubicin-based nano-drug delivery system in triple negative breast cancer. Frontiers in Bioengineering and Biotechnology. 2023;11():1271420. doi:10.3389/fbioe.2023.1271420

[19] Ansari Yaasir Ahmed, Farooque Mohd, Ahmad Anwar, Azhruddin Md, Sayyed M. Phytochemical Investigation Studies of Anti-Diabetic Phytochemicals of Plant Murraya Koenigii (Linn.) Spreng Belonging to Family Rutaceae. International Journal of Research in Advent Technology. 2019;7(4S):45-49.

[20] Yang W., Sun Q., Zhang X., et al. A novel doxorubicin/CTLA-4 blocker co-loaded drug delivery system improves efficacy and safety in antitumor therapy. Cell Death & Disease. 2024;15(6):386. doi:10.1038/s41419-024-06776-6

[21] Vinothini K., Dhilip Kumar S. S., Abrahamse H., et al. Enhanced Doxorubicin Delivery in Folate-Overexpressed Breast Cancer Cells Using Mesoporous Carbon Nanospheres. ACS Omega. 2021;6(50):34532-34545. doi:10.1021/acsomega.1c04820

[22] Yu J., Wang L., Xie X., et al. Multifunctional Nanoparticles Codelivering Doxorubicin and Amorphous Calcium Carbonate Preloaded with Indocyanine Green for Enhanced Chemo-Photothermal Cancer Therapy. International Journal of Nanomedicine. 2023;18():323-337. doi:10.2147/IJN.S394896

[23] Vahid Tajkhan, Ansari Yaasir Ahmed, Umme Rumana, Patel Afroza, Anwar Ahmad, Ansari Mohd Razi, Siddiqui Nameera Amreen. Studies on the Synthesis, Characterization, and Biological Activities of Some New Heterocyclic Moieties Containing 1,2,4-Triazoles. International Journal of Life Science and Pharma Research. 2020;Sp-12:4-9.

[24] Ng C. X., How C. W., Lee S. H. Precision-engineered PEGylated liposome for dual payload delivery: enhancing efficacy of Doxorubicin hydrochloride and miR-145 mimics in breast cancer cells. Journal of Liposome Research. 2025;35(1):15-28. doi:10.1080/08982104.2024.2385457

[25] Tseng H., Kuo C., Liao W., et al. Indocyanine green as a near-infrared theranostic agent for ferroptosis and apoptosis-based, photothermal, and photodynamic cancer therapy. Frontiers in Molecular Biosciences. 2022;9():1045885. doi:10.3389/fmolb.2022.1045885

[26] Ma R., Alifu N., Du Z., et al. Indocyanine Green-Based Theranostic Nanoplatform for NIR Fluorescence Image-Guided Chemo/Photothermal Therapy of Cervical Cancer. International Journal of Nanomedicine. 2021;16():4847-4861. doi:10.2147/IJN.S318678

[27] Liao W., Chang D., Lin M., et al. Indocyanine-Green-Loaded Liposomes for Photodynamic and Photothermal Therapies: Inducing Apoptosis and Ferroptosis in Cancer Cells with Implications beyond Oral Cancer. Pharmaceutics. 2024;16(2):224. doi:10.3390/pharmaceutics16020224

[28] Pan W., Chen W., Min Y., et al. ICG-Loaded PEG-Modified Black Phosphorus Nanosheets for Fluorescence Imaging-Guided Breast Cancer Therapy. ACS Omega. 2021;6(51):35505-35513. doi:10.1021/acsomega.1c04909

[29] Li Z., Sun L., Lan J., et al. Illuminating the fight against breast cancer: Preparation and visualized photothermal therapy of hyaluronic acid coated ZIF-8 loading with indocyanine green and cryptotanshinone for triple-negative breast cancer. Materials Today Bio. 2024;28():101200. doi:10.1016/j.mtbio.2024.101200

[30] Lekmeechai S., Pietras K., Axelsson O. 177Lu−SN201 nanoparticle shows superior anti−tumor efficacy over conventional cancer drugs in 4T1 orthotopic model. Investigational New Drugs. 2024;42(4):471-477. doi:10.1007/s10637-024-01450-2

[31] Linde C., Chien Y., Chen Z., et al. Nanoparticle-enhanced PD-1/PD-L1 targeted combination therapy for triple negative breast cancer. Frontiers in Oncology. 2024;14():1393492. doi:10.3389/fonc.2024.1393492

[32] Guo K., Sun Y., Xiong H. The Application of Nanomaterials in Breast Cancer. Pharmaceutics. 2025;17(12):1608. doi:10.3390/pharmaceutics17121608

[33] Wang R., Kumar P., Reda M., et al. Nanotechnology Applications in Breast Cancer Immunotherapy. Small. 2023;():2308639. doi:10.1002/smll.202308639

[34] Pande S. Factors affecting response variables with emphasis on drug release and loading for optimization of liposomes. Artificial Cells, Nanomedicine, and Biotechnology. 2024;52(1):334-344. doi:10.1080/21691401.2024.2360634

[35] Asif A., Desu P., Alavala R., et al. Development, Statistical Optimization and Characterization of Fluvastatin Loaded Solid Lipid Nanoparticles: A 32 Factorial Design Approach. Pharmaceutics. 2022;14(3):584. doi:10.3390/pharmaceutics14030584

[36] Kurmi B. D., Paliwal S. R. Development and optimization of TPGS-based stealth liposome of doxorubicin using Box-Behnken design: characterization, hemocompatibility, and cytotoxicity evaluation in breast cancer cells. Journal of Liposome Research. 2022;32(2):129-145. doi:10.1080/08982104.2021.1903034